Trajectory Modeling of Gas–Liquid Flow in Microchannels with Stochastic Differential Equation and Optical Measurement

Lexiang Zhang, Feng Xin, Dongyue Peng, and Weihua Zhang
School of Chemical Engineering and Technology, Tianjin University, Tianjin 300072, China

Collaborative Innovation Center of Chemical Science and Engineering (Tianjin), Tianjin 300072, China

Yuexing Wang, Xiaodong Chen, and Yi Wang
Key Laboratory of Opto-Electronics Information Technology of Ministry of Education, College of Precision Instrument and Opto-Electronics Engineering, Tianjin University, Tianjin 300072, China

DOI 10.1002/aic.14938
Published online July 14, 2015 in Wiley Online Library (wileyonlinelibrary.com)

The numbering-up of microchannel reactors definitely faces great challenge in uniformly distributing fluid flow in every channel, especially for multiphase systems. A model of stochastic differential equations (SDEs) is proposed based on the experimental data recorded by a long-term optical measurement to well quantify the stochastic trajectories of gas bubbles and liquid slugs in parallel microchannels interconnected with two dichotomic distributors. The expectation and variance of each subflow rate are derived explicitly from the SDEs associated with the Fokker–Planck equation and solved numerically. A bifurcation in the trajectory is found using the original model, then a modification on interactions of feedback and crosstalk is introduced, the evolutions of subflow rates calculated by the modified model match well with experimental results. The established methodology is helpful for characterizing the flow uniformity and numbering-up the microchannel reactors of multiphase system. © 2015 American Institute of Chemical Engineers *AIChE J*, 61: 4028–4034, 2015
Keywords: stochastic differential equation, gas–liquid flow, parallel microchannels, optical measurement, numbering-up

Introduction

Numbering-up or scaling-out of multiple microchannels by repetition is the fundamental strategy for microreactor approaching commercial throughputs to enlarge the benefits emerging from small scale.[1,2] The serious challenges that should be well addressed are to understand the coupling among microchannels and guarantee uniform distribution in each and every microchannel when fluids pass through.

But gas–liquid distribution in parallel microchannels involves a complicated mechanism driven by local pressure distribution, gas compressibility, and even noise from inputs. Such an intricate interaction appears randomly and results in stochastic flow variance. Abate and Weitz.[3] used serial splitting arrays to realize multiple emulsions, the drops could either choose one path, remaining intact, or follow both paths, splitting in two at junctions. Yue et al.[4] captured disordered slug sizes in 16 microchannels with two constructal distributors. The irregularity of bubble sizes was also found and counted in their multiply microchannels by external numbering-up.[5] Chen et al.[6] observed random alternation of free channels and blocked channels in comb-like parallel microchannels of gas–liquid flow.

Correspondence concerning this article should be addressed to F. Xin at xinf@tju.edu.cn.

A number of correlations had been established to empirically describe size and frequency of bubble emergence,[7,8] such as Garstecki's linear relationship of bubble length and the ratio of flow rates,[9] they are deterministic for estimating the average. Actually, the transient variance must be quantified by stochastic equations for obtaining statistic characteristics. Subsequently, the indeterminateness of random process has to be tested by a long term operation, where bifurcation[10] even chaos may occur.

Stochastic Differential Equation (SDE) has been popular for modeling diverse random behaviors in finance, engineering, economics, and epidemiology, such as fluctuation of stocks and state estimation in process monitor and control.[11–15] In our work, SDEs are constructed to formulize the instantaneous distribution of gas and liquid flows in double microchannels by introducing a diffusion term to imitate the variability.

Parameters in SDE are usually estimated by sampling,[16] whose amount determines the accuracy of the estimation, the conventional imaging technique is not sufficient to collect and analyze a huge amount of information on flows and distribution. Therefore, we developed an optical measurement system to avoid the problems in image treatment, such as limitation in storage capacity of charge coupled device (CCD) camera and uncertainties in discerning edges and sizes on blurred gas–liquid interface,[17] because of exceptional fast response of our home-made system.

Randomness of two-phase flows would result in multiformity of sizes of bubble and slug in each and every microchannel,

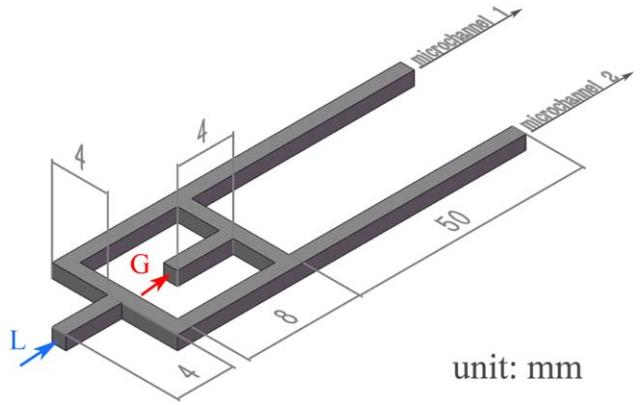

Figure 1. Structure of the microchannels.

[Color figure can be viewed in the online issue, which is available at wileyonlinelibrary.com.]

furthermore influence reaction performance and make trouble in numbering-up. Despite some concepts on reducing variations and achieving uniform distribution have been conceived, such as introducing pressure barrier channels,[18] the flow and distribution behavior of multiphase in microchannels is still poorly understood. The vision of a large-scale microreactor is not out of reach as long as the maldistribution of fluids is acceptable or describable. Therefore, our aim is to quantify the uncertainty in numbering-up with stochastic model. SDEs could predict probabilities of trajectories of multiphase flows developing in future. Here, the most representative structure of two T-junction microchannels in parallel is studied.

Experiment

The microchannels were fabricated on a polymethyl methacrylate (PMMA) substrate plate by precisely processing and sealed by another PMMA cover plate. All channels of parallel microchannels and distribution channels had the same square cross section of 500 μm by 500 μm. The detailed dimensions are specified in Figure 1. The experiments were conducted in ambient condition, air and deionized water were chosen as gas and liquid phases. Both fluid streams were bifurcated into two symmetric subchannels through a dichotomic distributor, slug flows were formed and passed through two microchannels after air and water contacted at T-junctions.

Figure 2a shows the experimental setup with the optical measurement system. The laser of 1550 nm and 70 mW generated by a semiconductor laser passed through an optical splitter of Huawei SPL9101-P104-SC/UPC and was split into four beams. Two adjacent fibers of C-Lens of SMF-28 with a maximum beam diameter of 0.5 mm were installed as closely as possible along each microchannel, and the four optical fibers were arranged as shown in Figure 2b. The laser transmitted across the transparent PMMA plate was received by a photodetector of LSIPD-L1 aligned on the opposite side of microchannel, where four photodetectors were connected in a parallel circuit for collecting and interpreting lights to electric signals. A data acquisition card of Art-Control PCI8532 transferred the electric signals to a computer with a sampling speed over 5 MHz for each path.

The experimental procedure included filling water with a syringe pump (Harvard Apparatus, PHD 22/2000) before air was pumped in, and stabilizing the slug flow for 2 min, then the signals were captured for about 10 min. Lengths and velocities of bubbles and liquids were calculated by a program of Visual BASIC. In the calculation program, a threshold of signal was chosen to distinguish air and water according to their difference in light transmittance. The instantaneous velocity of a bubble or a slug was calculated through distance between two optical fibers over one microchannel and time interval of one bubble or slug passing such a distance. Their lengths were calculated by velocities and experiencing time exampled in Figure 3a.

Results

Flow patterns and signals

In our experimental conditions, three typical patterns of bubbly, slug, and slug-annular flows were observed, stratified flow and channeling phenomena occasionally appeared. A proper interpretation of the signal and inference of the flow pattern is discussed.

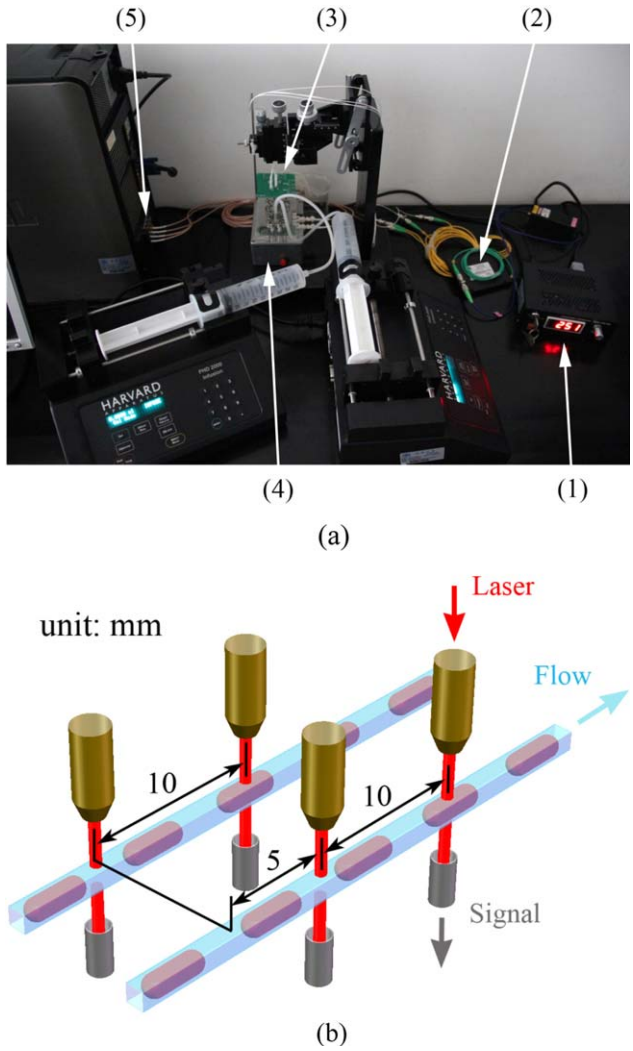

Figure 2. (a) Experimental setup with optical detection: (1) laser source; (2) optical splitter; (3) multiply optical fibers; (4) photodectors; (5) data acquisition card. (b) Arrangement of optical fibers.

[Color figure can be viewed in the online issue, which is available at wileyonlinelibrary.com.]

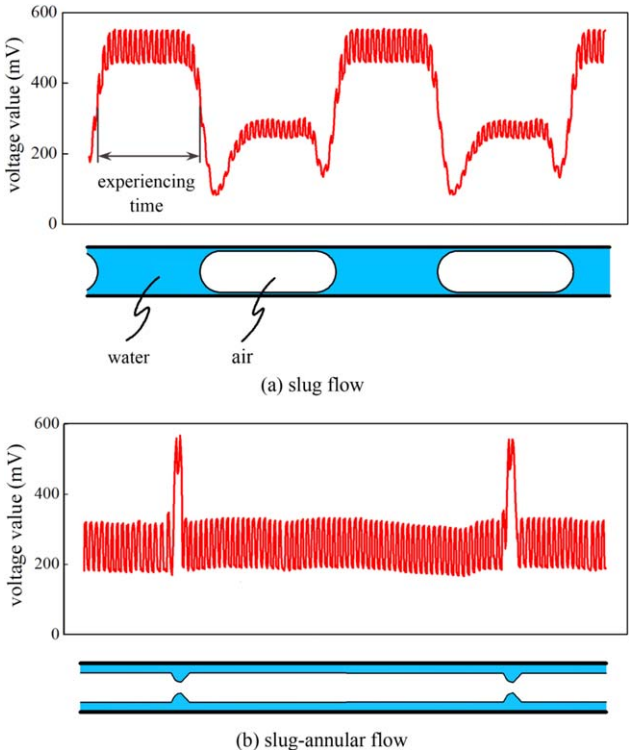

Figure 3. Schematic signals of two typical flow patterns.

[Color figure can be viewed in the online issue, which is available at wileyonlinelibrary.com.]

When bubbles and liquid slugs passed through the optical fibers under slug flow pattern, the signals recorded by computer are shown in Figure 3a. The high and low voltages represent the water slug and air bubble, respectively. The noise was caused by the pulse of laser.

In the slug-annular flow as shown in Figure 3b, a gas core is surrounded by a liquid film where large-amplitude solitary waves appear and small slugs are sometimes present.[19] The intensities of voltage signals are between those of bubble and slug in slug flow, large fluctuations respond to the slugs and ring-shaped waves in the film.

Distribution of flow rates

Reasonably characterizing flow uniformity should be based on precisely describing trajectories of flow rate in every microchannel, rather than the accumulative flow rates measured at outlet, nor total flow rate of gas or liquid input. Accordingly, calculation equations of the transient flow rates based on the optical measurement were derived.

When Capillary number in rectangular microchannel is lower than 0.1, the cross section of bubbles is nonaxisymetrical and square-like. One bubble can be described approximately as a body of pseudo cylinder with square-like cross section and rounded corners between two hemispherical caps, whose geometry is plotted in Figure 4a. Equations 1–5 were for calculating the volumes of bubble and slug in one unit cell, including one bubble, one adjacent slug, and surrounded liquid film.[20] The thickness of liquid film was estimated by the correlation of Kolb and Cerro[21]

$$V_B = V_{2caps} + V_{body} = \frac{\pi}{6}(w - 2L_{film})^3 + (1 - W')w^2 L_{body} \quad (1)$$

$$W' = \frac{4L_{film}}{w}\left(1 - \frac{L_{film}}{w}\right) + \frac{4-\pi}{w^2}\left(\frac{w}{4} - \frac{L_{film}}{2}\right)^2 \quad (2)$$

$$L_{body} = L_B - w + 2L_{film} \quad (3)$$

$$L_{film} = 0.003 \cdot w \quad (4)$$

$$V_L = V_{uc} - V_B = (L_B + L_s)w^2 - V_B \quad (5)$$

Let the flow rates of gas and liquid in microchannels 1 and 2 be denoted by q_{G1}, q_{L1}, q_{G2}, and q_{L2}, respectively. If q_i was unchanged in bubble formation stage, they could be calculated by volumes of two phases in one unit cell and their emergence frequencies

$$q_i = V_i \cdot f_i,\ i = \text{G1, G2, L1, and L2} \quad (6)$$

Figure 4b exampled one set of calculated subflow and total flow rates of gas phase varying with time. Although the total flow rates of feeds were unchanged by pump settings, the calculated total flow rates were transient and changed due to the compressibility of air. The distance shift of 5 mm between optical fibers in double microchannels showed in Figure 2b was considered by shifting time scale. The oscillations of q_{G1},

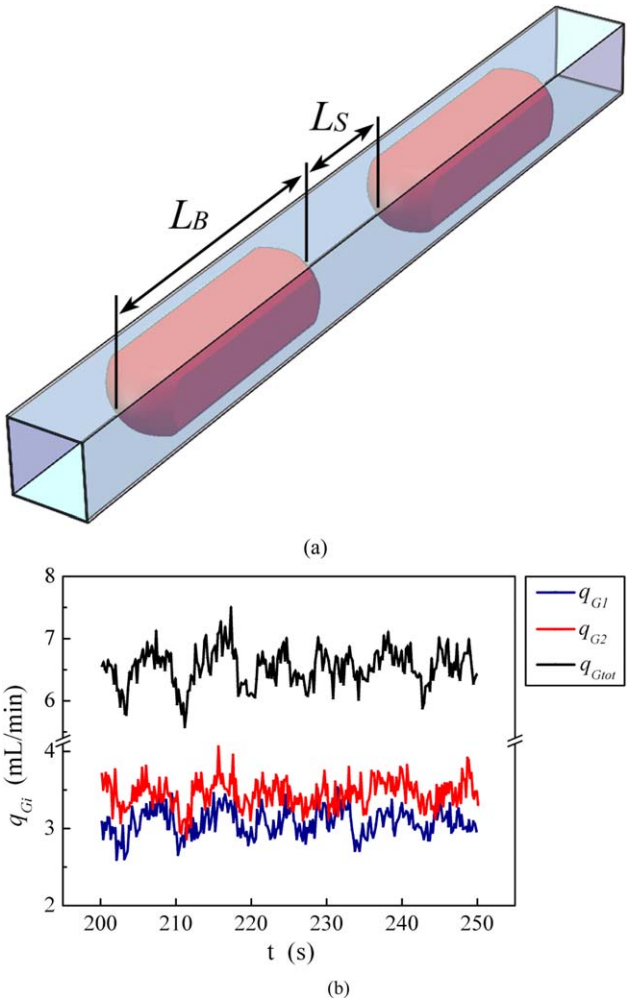

Figure 4. (a) A three-dimensional schematic geometry of unit cell in slug flow. (b) Calculated transient sub and total flow rates of air at $q_{Gtot} = q_{Ltot} = 6$ mL/min.

[Color figure can be viewed in the online issue, which is available at wileyonlinelibrary.com.]

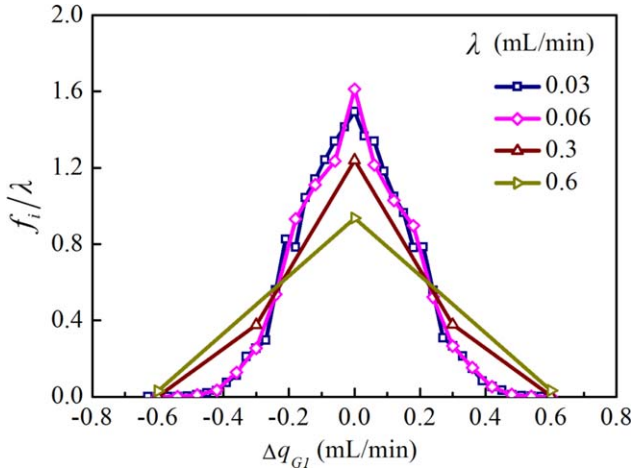

Figure 5. The effect of interval size λ on the profile of Δq_{G1} at a typical sampling of 600 s at $q_{Gtot} = q_{Ltot} = 6$ mL/min.

[Color figure can be viewed in the online issue, which is available at wileyonlinelibrary.com.]

q_{G2}, and q_{Gtot} periodically appeared in Figure 4b could be attributed to the syringe pumps and crosstalk between microchannels. The calculated total flow rates of gas and liquid were 9 −12% more than setting values of pumps, respectively, due to the simplified algorithm.

Stochastic model

The variability of subflow rates is stochastic and describable with statistic eigenvalues deduced from SDE. Establishing of SDE for each subflow rate is similar, taking q_{G1} at $q_{Gtot} = q_{Ltot} = 6$ mL/min as illustration.

We defined the gas flow rate in microchannel 1 q_{G1} as the elementary event, which belonged to the interval from 0 to q_{Gtot}, and a set of all possible q_{G1} constituted the sample space. We assumed the variations of subflow rates were four independent events, the feedbacks and crosstalks between microchannels were ignored. The continuous stochastic process of subflow rate was defined on such probability space.[22]

The model was first developed by studying for a small time interval Δt. Let $q_{G1}(t)$ represents the subflow rate of gas in microchannel 1 at time t, and Δq_{G1} be the change in Δt. For Δt, the infinite possible state changes of continuous random variable Δq_{G1} were expressed by finite intervals of equal size. Each interval $[x_1, x_2]$ was represented by the central value $\frac{x_1+x_2}{2}$, and its appearance times N_i was counted from a sample. The average occurrence frequency f_i is defined as N_i averaged in 1 s, and interval size of $\lambda = x_2 - x_1$ would affect distribution of the series of f as shown in Figure 5. When λ was less than 0.06 mL/min, the change of profile was inappreciable. Trading off the parameter number and the accuracy, λ = 0.06 mL/min was used in this work.

It is assumed that Δt is sufficiently small and at most one change can occur in Δt and neglected multiple change which have probabilities of order $(\Delta t)^2$. Twenty-four possible changes of q_{G1} in Δt along with corresponding probabilities are listed in Table 1. For example, change 12 represents a decrease of 0.06 mL/min when a new bubble emerged, whose probability equals the product of Δt and average occurrence frequency f_{12}. Change 13 includes two cases of no new bubble produced, and a new bubble formed with q_{G1} varying less than 0.03 mL/min.

Table 1. Possible Changes with Corresponding Probabilities

I	State Change Δq_{G1} (mL/min)	Probability
1	−0.72	$P(1) = f_1 \Delta t$
2	−0.66	$P(2) = f_2 \Delta t$
...	...	...
12	−0.06	$P(12) = f_{12} \Delta t$
13	0	$P(13) = 1 - \sum_{i=1}^{12} P(i) - \sum_{j=14}^{24} P(j)$
14	0.06	$P(14) = f_{14} \Delta t$
...	...	...
23	0.60	$P(23) = f_{23} \Delta t$
24	0.66	$P(24) = f_{24} \Delta t$

The twenty-three parameters of f_i in Table 1 were statistically determined from an experimental sample. The sampling size independence test has been done by comparing the q_{G1} distributions from different sampling size of 10, 600, and 1000 s in Figure 6. Usually, a fast camera recorded only 10 s at a time. The sampling size of 600 s was used in this article with which a representative distribution could be achieved and the accuracy would not improve obviously with the increase of size. All the f_i in Table 1 were used by the values of magenta curve in Figure 5 multiplying λ of 0.06 mL/min.

Using Table 1, the expectation and covariance of Δq_{G1} were calculated

$$E(\Delta q_{G1}) = \sum_{j=1}^{24} P(j) \Delta q_{G1,j} \tag{7}$$

$$E\left[(\Delta q_{G1})^2\right] = \sum_{j=1}^{24} P(j) \Delta q_{G1,j} \Delta q_{G1,j} \tag{8}$$

Notice that as Δt was small and $E(\Delta q_{G1})E(\Delta q_{G1})$ was on the order of $(\Delta t)^2$, the covariance was set equal to $E(\Delta q_{G1} \Delta q_{G1})$. It is well-known that the drift and diffusion coefficients, g and k of the SDE, are equal to the expectation of Δq_{G1} divided by Δt and the square root of the covariance of Δq_{G1} divided by Δt, respectively[23]

$$g = E(\Delta q_{G1})/\Delta t \tag{9}$$

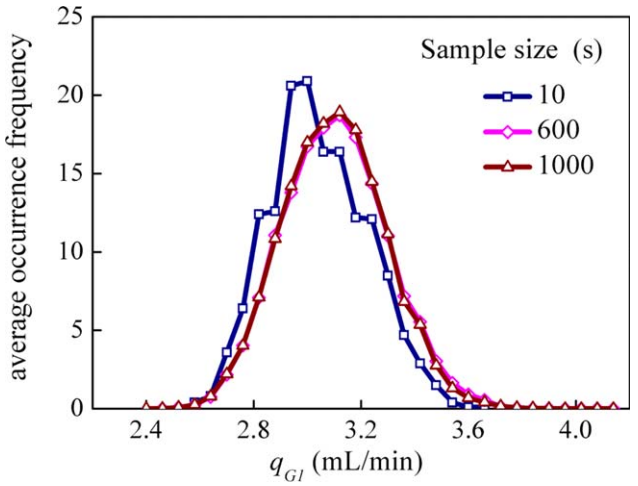

Figure 6. Variation of q_{G1} in different sampling sizes.

[Color figure can be viewed in the online issue, which is available at wileyonlinelibrary.com.]

Table 2. Parameters in SDEs of Subflow Rates

	g (mL/min^{-1} s^{-1})	k (mL/min^{-1} s$^{-0.5}$)
q_{G1}	-9.934×10^{-4}	5.960×10^{-4}
q_{L1}	-1.192×10^{-3}	8.583×10^{-4}
q_{G2}	9.934×10^{-4}	5.960×10^{-4}
q_{L2}	1.149×10^{-3}	1.048×10^{-3}

$$k=\sqrt{E(\Delta q_{G1}\Delta q_{G1})/\Delta t} \tag{10}$$

An Itô form SDE is obtained as the time interval approaches to zero

$$dq_{G1}=gdt+kdW(t) \tag{11}$$

$W(t)$ is the Wiener process with zero mean and unit variance. The second differential on the right-side is the source of uncertainty, Eq. 11 is reduced to a deterministic model if set k to zero. Furthermore, equations analogous to Eq. 11 were proposed for each subflow rate, and the coefficients are listed in Table 2.

Exact solution of SDE is generally difficult to obtain, and Euler–Maruyama approximation[24] for numerical solution has the iterative scheme

$$(q_{G1})_{n+1}=(q_{G1})_n+g\Delta t+k\sqrt{t_{n+1}-t_n}N \tag{12}$$

The term $\sqrt{t_{n+1}-t_n}N$ is an approximation of the Wiener process increment over time step t_n to t_{n+1}, which was performed by a customized MATLAB algorithm using random number generator randn.

A sample path of the solution mimics the random evolution of subflows. Every time the computation path was occasional and different though governed by the identical statistic characteristic, this is accorded with the indeterminateness in practice. Three individual paths and the mean over 10,000 sample paths of $q_{G1}(t)$ are plotted in Figure 7 when the initial value is 3 mL/min. Simulations indicate that SDE models are good at portraying the manner of randomness.

Eigenvalues from SDE

SDE is easy to simulate and offers certain theoretical insights. Description of flow uniformity of gas–liquid two phases in branches and quantifying what behaviors the system will generate in future are of interest. Expectation and variance of subflow rates, parameters that could characterize the distribution of gas and liquid, were chosen as a criterion.

The expectation and variance of a continuous random variable x are defined by

$$E(x)=\int_{-\infty}^{\infty} xp(x)dx \tag{13}$$

$$\sigma^2(x)=\int_{-\infty}^{\infty}(x-E(x))^2p(x)dx=\int_{-\infty}^{\infty}x^2p(x)dx-E(x)^2 \tag{14}$$

The Fokker–Planck equation of Eq. 15 describes the time evolution of probability density function $p(t, x)$. Two boundary conditions were given in the form of Dirac delta function δ, and x_0 is the initial value of SDE at time zero

$$\begin{cases}\dfrac{\partial p(t,x)}{\partial t}=-\dfrac{\partial(gp(t,x))}{\partial x}+\dfrac{k^2}{2}\dfrac{\partial^2(p(t,x))}{\partial x^2}\\ p(0,x)=\delta(x-x_0)\end{cases} \tag{15}$$

The analytical solution to this equation is[23]

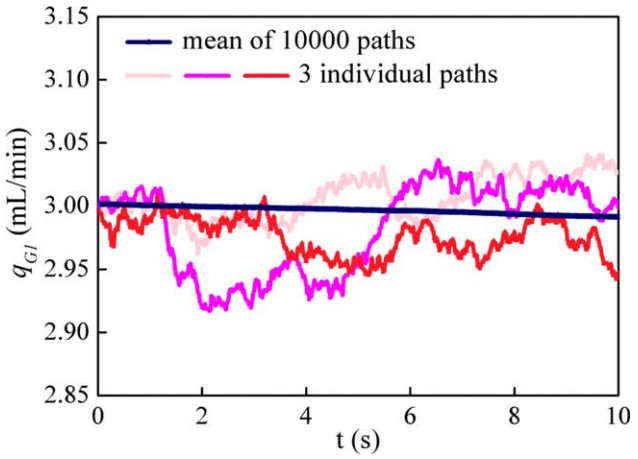

Figure 7. Numerical approximation of Eq. 11 averaged over 10,000 paths and three exampled paths.

[Color figure can be viewed in the online issue, which is available at wileyonlinelibrary.com.]

$$p(t,x)=\frac{1}{\sqrt{2\pi k^2 t}}\exp\left[\frac{-(x-gt-x_0)^2}{2k^2t}\right] \tag{16}$$

Letting $a=\frac{1}{\sqrt{2\pi k^2 t}}$, $b=gt+x_0$, and $c=2k^2t$. Substituting Eq. 16 to Eq. 13 and integrating give the explicit expression for expectation of each subflow rate

$$E(q_i(t))=\frac{ac}{2}\exp\left(-\frac{b^2}{c}\right)+\frac{ab\sqrt{\pi c}}{2}\left[1+\mathrm{erf}\left(\frac{b}{\sqrt{c}}\right)\right], \tag{17}$$
$$i=\ \mathrm{G1,\ G2,\ L1,\ or\ L2}$$

The error function erf, encountering in integrating the normal distribution, is defined by

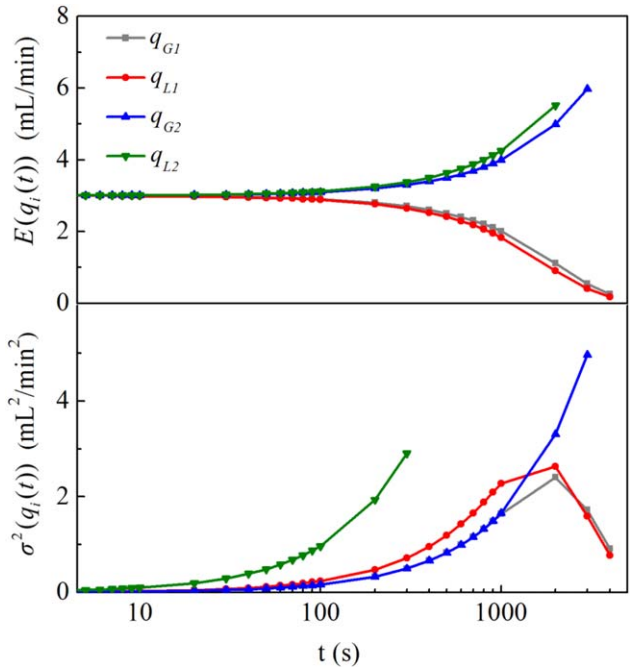

Figure 8. Calculated $E(q_i(t))$ and $\sigma^2(q_i(t))$ variation at $q_{Gtot}=q_{Ltot}=6$ mL/min. The initial values were set as an equipartition of 3 mL/min.

[Color figure can be viewed in the online issue, which is available at wileyonlinelibrary.com.]

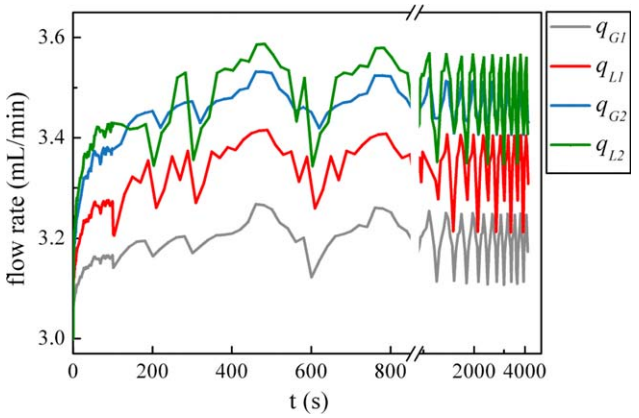

Figure 9. 500 paths mean trajectories of subflow rates at $q_{Gtot} = q_{Ltot} = 6$ mL/min. The initial values were set as an equipartition of 3 mL/min.

[Color figure can be viewed in the online issue, which is available at wileyonlinelibrary.com.]

$$\mathrm{erf}(x) = \frac{2}{\sqrt{\pi}} \int_0^x e^{-y^2} dy \tag{18}$$

Also, the exact expression for variance could be derived from Eqs. 14 and 16

$$\sigma^2(q_i(t)) = -\frac{abc}{2} \exp\left(-\frac{b^2}{c}\right) + \frac{a\sqrt{\pi c}(c-2b^2)}{4}\left[1+\mathrm{erf}\left(\frac{b}{\sqrt{c}}\right)\right] + 2bE[q_i(t)] - E(q_i(t))^2, \quad i = \mathrm{G1},\ \mathrm{G2},\ \mathrm{L1},\ \text{or}\ \mathrm{L2} \tag{19}$$

Figure 8 presents evolution of expectation and variance of four subflow rates calculated by Eqs. 17 and 19, respectively. Simulated distribution tends to polarization that $E(q_{G1})$ and $E(q_{L1})$ approaches zero after approximately 3500 s. Also $\sigma^2(q_{G1})$ and $\sigma^2(q_{L1})$ decreased after an enlargement of 2000 s. Gas and liquid both preferred running in microchannel 2 and extinctions in microchannel 1, this deviation was accorded with the previous flow uniformity research which was interpreted as the fabrication difference between microchannels.[25] But stagnation in microchannel 1 does not come up in practice due to the significant crosstalk and feedback in the system that larger amount of fluids running into either channel usually increases its pressure drop, then the fluids tend to compensate to another branch.

Persistence time of t_P is defined as the time until any of subflows drains away. For the deterministic model, the persistence time is always infinite. However, t_P is likely to be finite if the random nature is taken into account. Simulation of SDEs is terminated when $E(q_i(t)) = 0$. In other words, slug flow was developing spatially in a solo microchannel after a period of operation, and the numbering-up was not achieved in a stable way. Channeling might appear temporarily according to pressure distribution.

Model modification

It is more accurate to modify by taking interactions between microchannels into consideration. The probabilities would be functions of pressure drops of two branches, while the transient pressure drops were difficult to estimate. A rough approximation to account pressure drop was replaced it by flow rate according to experiment phenomenon that each subflow rate stabilized around some value. Hence, a new form of probabilities was assumed that the 23 parameters of f_i in Table 1 were modified as the Gauss function of its subflow rate, $P(i) = f_i(q_{G1})\Delta t$, so that the probabilities of moving closer to the stabilized interval were greater than those of moving further away.

Using the same sample above, the mean trajectories of 500 paths from new-formed SDEs were plotted in Figure 9. The mean flow rates checked and balanced around 3.1–3.5 mL/min, conforming to the case in Figure 4b. The overestimation of phase flow rates to feedings was due to the simplification algorithm of subflow rate. As the two phases experienced instantaneous flow stagnations alternately when formed slug flow at T-junctions, it is common that neither of two phases in microchannels could meet mass balance to pump settings in a small time scale.

These results exemplified a proper way to quantify the stochastic system and the comparison provided valuable insights into interplays through parallel microchannels. The interaction is related to the length of distribution channels as long distance between microchannels weakens their crosstalk, such situation may appear instable distribution and could be described by the original model.

Conclusion

Stochastic phenomenological models, with and without considering the interaction between microchannels, have been developed for the description of the fluids of gas and liquid distribution in parallel microchannels. A long-term measurement of optical system with a fast sampling speed was built to continually monitor the messages from parallel slug flows, sampling for parameters estimation. Analytical expressions of expectation and variance of subflow rates were deduced mathematically by the SDEs and Fokker–Planck equation, and simulations have covered a possible bifurcation in trajectories when interplays between microchannels could be ignored. A modified model based on significant crosstalk and feedback between microchannels matches well with experiment. All of the findings will facilitate numbering-up the microchannels reactor for gas–liquid flow. Characterizing of the fluids distribution in larger number of microchannels by this fashion could attempt to be analogized from above models.

Acknowledgments

The authors gratefully acknowledge the support of the National Natural Science Foundation of China (NSFC 21276180).

Notation

a, b, c = parameter
E = expectation
f = frequency, Hz
g = parameter, mL/min s
k = parameter, mL/min $s^{0.5}$
L = length, mm
N = Gaussian distribution with zero mean and unit variance
N_i = occurrence time of event i
$P(i)$ = probability of event i, dimensionless
$p(x)$ = probability density function
q = flow rate, mL/min
Δq = flow rate change, mL/min
V = volume, mL
W = Wiener process, dimensionless

W' = fraction of the cross section of a channel remaining for the gutters and the film, dimensionless
w = width of square cross section of microchannels, mm
x_0 = initial value

Greek letters

λ = interval size of the flow rate change, mL/min
σ^2 = variance
δ = Dirac delta function

Subscripts

B = bubble
body = body of the bubble
cap = cap of the bubble
film = liquid film
G = gas
L = liquid
P = persistent
S = slug
tot = total
uc = a unit cell of slug flow
1 = microchannel 1
2 = microchannel 2

Literature Cited

1. de Mas N, Gunther A, Kraus T, Schmidt MA, Jensen KF. Scaled-out multilayer gas-liquid microreactor with integrated velocimetry sensors. *Ind Eng Chem Res*. 2005;44:8997–9013.
2. Mills PL, Quiram DJ, Ryley JF. Microreactor technology and process miniaturization for catalytic reactions—a perspective on recent developments and emerging technologies. *Chem Eng Sci*. 2007;62:6992–7010.
3. Abate AR, Weitz DA. Faster multiple emulsification with drop splitting. *Lab Chip*. 2011;11:1911–1915.
4. Yue J, Boichot R, Luo L, Gonthier Y, Chen G, Yuan Q. Flow distribution and mass transfer in a parallel microchannel contactor integrated with constructal distributors. *AIChE J*. 2009;56:298–317.
5. Romanowsky MB, Abate AR, Rotem A, Holtze C, Weitz DA. High throughput production of single core double emulsions in a parallelized microfluidic device. *Lab Chip*. 2012;12:802–807.
6. Chen J, Wang S, Cheng S. Experimental investigation of two-phase distribution in parallel micro-T channels under adiabatic condition. *Chem Eng Sci*. 2012;84:706–717.
7. Sullivan MT, Stone HA. The role of feedback in microfluidic flow-focusing devices. *Philos Trans R Soc A*. 2008;366:2131–2143.
8. Glawdel T, Elbuken C, Ren CL. Droplet formation in microfluidic T-junction generators operating in the transitional regime. II. Modeling. *Phys Rev E*. 2012;85(1):1–12.
9. Garstecki P, Fuerstman MJ, Stone HA, Whitesides GM. Formation of droplets and bubbles in a microfluidic T-junction—scaling and mechanism of break-up. *Lab Chip*. 2006;6:437–446.
10. Elnashaie SSEH, Grace JR. Complexity, bifurcation and chaos in natural and man-made lumped and distributed systems. *Chem Eng Sci*. 2007;62:3295–3325.
11. Allen LJS, Allen EJ. A comparison of three different stochastic population models with regard to persistence time. *Theor Popul Biol*. 2003;64:439–449.
12. Hull J, White A. The pricing of options on assets with stochastic volatilities. *J Finance*. 1987;2:281–300.
13. Yuan Y, Allen LJS. Stochastic models for virus and immune system dynamics. *Math Biosci*. 2011;234:84–94.
14. Hayes JG, Allen EJ. Stochastic point-kinetics equations in nuclear reactor dynamics. *Ann Nucl Energy*. 2006;32:572–587.
15. Lima FV, Rawlings JB. Nonlinear stochastic modeling to improve state estimation in process monitoring and control. *AIChE J*. 2011;57:996–1007.
16. Bishwal JPN. *Parameter Estimation in Stochastic Differential Equations*. Berlin: Springer-Verlag, 2008:15–118.
17. Ide H, Kimura R, Kawaji M. Optical measurement of void fraction and bubble size distributions in a microchannel. *Heat Transf Eng*. 2007;28:713–719.
18. Al-Rawashdeh M, Nijhuis X, Rebrov EV, Hessel V, Schouten JC. Design methodology for barrier-based two phase flow distributor. *AIChE J*. 2012;58:3482–3493.
19. Shao N, Gavriilidis A, Angeli P. Flow regimes for adiabatic gas-liquid flow in microchannels. *Chem Eng Sci*. 2009;64:2749–2761.
20. Leclerc A, Philippe R, Houzelot V, Schweich D, de Bellefon C. Gas-liquid Taylor flow in square micro-channels: new inlet geometries and interfacial area tuning. *Chem Eng J*. 2010;165:290–300.
21. Kolb WB, Cerro RL. Coating the inside of a capillary of square cross section. *Chem Eng Sci*. 1991;46:2181–2195.
22. Øksendal B. *Stochastic Differential Equations*, 5th ed. Berlin: Springer-Verlag, 2000:7–14.
23. Allen E. *Modeling with Itô Stochastic Differential Equations*. Berlin: Springer-Verlag, 2007:89–153.
24. Higham DJ. An algorithmic introduction to numerical simulation of stochastic differential equations. *SIAM Rev*. 2011;43:525–546.
25. Zhang L, Peng D, Lyu W, Xin F. Uniformity of gas and liquid two phases flowing through two microchannels in parallel. *Chem Eng J*. 2015;263:452–460.

Manuscript received Mar. 19, 2015, and revision received May 14, 2015.